PNAS RESEARCH ARTICLE | CELL BIOLOGY

Impaired end joining induces cardiac atrophy in a Hutchinson–Gilford progeria mouse model

Yu Chen[a,b,1], Shiqi Huang[c,1], Zhen Cui[a,b], Xiaoxiang Sun[a,b], Yansong Tang[c], Hongjie Zhang[c], Zhixi Chen[a,b], Rui Jiang[c], Weina Zhang[a,b], Xue Li[c], Jiayu Chen[a,b], Baohua Liu[d], Ying Jiang[a,b], Ke Wei[c,2], and Zhiyong Mao[a,b,e,2]

Edited by James Cleaver, University of California, San Francisco, CA; received June 6, 2023; accepted October 14, 2023

Patients with Hutchinson–Gilford progeria syndrome (HGPS) present with a number of premature aging phenotypes, including DNA damage accumulation, and many of them die of cardiovascular complications. Although vascular pathologies have been reported, whether HGPS patients exhibit cardiac dysfunction and its underlying mechanism is unclear, rendering limited options for treating HGPS-related cardiomyopathy. In this study, we reported a cardiac atrophy phenotype in the *Lmna*$^{G609G/G609G}$ mice (hereafter, HGPS mice). Using a GFP-based reporter system, we demonstrated that the efficiency of nonhomologous end joining (NHEJ) declined by 50% in HGPS cardiomyocytes in vivo, due to the attenuated interaction between γH2AX and Progerin, the causative factor of HGPS. As a result, genomic instability in cardiomyocytes led to an increase of CHK2 protein level, promoting the LKB1-AMPKα interaction and AMPKα phosphorylation, which further led to the activation of FOXO3A-mediated transcription of atrophy-related genes. Moreover, inhibiting AMPK enlarged cardiomyocyte sizes both in vitro and in vivo. Most importantly, our proof-of-concept study indicated that isoproterenol treatment significantly reduced AMPKα and FOXO3A phosphorylation in the heart, attenuated the atrophy phenotype, and extended the mean lifespan of HGPS mice by ~21%, implying that targeting cardiac atrophy may be an approach to HGPS treatment.

Hutchinson–Gilford progeria syndrome | cardiac atrophy | DNA repair | nonhomologous end joining | aging

HGPS is a rare premature aging syndrome caused by a single point mutation, G608G, in the human *LMNA* gene (G609G in the mouse *Lmna* gene), leading to the accumulation of Progerin, the disease-causing mutant form of the Lamin A protein (1, 2). According to the Progeria Research Foundation, the mean lifespan of HGPS patients is approximately 14.5 y. HGPS patients develop cardiovascular diseases, as evidenced by phenotypes associated with atherosclerosis, and predominantly die because of heart failure, myocardial infarction, and stroke (3). Several studies have explored the mechanisms underlying the vascular pathologies in HGPS (4, 5). However, whether and how Lamin A mutation directly causes heart dysfunction remains to be investigated in order to develop potential approaches to treat cardiac abnormalities in HGPS.

The rise in genomic instability is a hallmark of aging (6). While no significant differences were observed in the accumulation of single nucleotide variants in the hearts of HGPS mice (7), it is important to note that both HGPS mice and human HGPS cells display increased genomic instability and heightened sensitivity to DNA damage inducers, particularly those that cause double-strand breaks (DSBs) (8, 9). These findings suggest that the accumulation of Progerin might result in impaired DSB repair in HGPS. Homologous recombination (HR) impairment in HGPS cells and *Lmna*-depleted cells has been well documented, while the alteration of nonhomologous end joining (NHEJ) remains contradictory in the literature (4, 8–10). These studies indicate that the dysregulation of NHEJ in HGPS may be context-dependent, and further clarification is needed to fully understand this aspect.

Defects in DSB repair contribute to cellular senescence or apoptosis (11, 12), but the connections between DSB repair alterations and tissue homeostasis have not been extensively studied. In the case of cardiomyocytes, whether Progerin leads to changes in NHEJ, the dominant DSB repair pathway in postmitotic cells, and whether such changes contribute to heart dysfunction in HGPS are still not well understood. The lack of an appropriate tool for studying the change in NHEJ in vivo is the major obstacle that hampers one from addressing the critical question. We previously developed an NHEJ reporter mouse model, R26NHEJ (13), for ex vivo NHEJ efficiency analysis. However, the assay requires isolating and culturing cells and introducing vectors expressing the I-SceI endonuclease to induce DSBs. Due to the technical challenges associated with isolating and

Significance

Cardiovascular compromise is the leading cause of death in patients with Hutchinson–Gilford progeria syndrome (HGPS). Although the mechanisms of vascular pathologies are documented, how heart dysfunctions develop in HGPS patients remains elusive. Here, we reported a phenotype of cardiac atrophy and a defect in DNA repair in HGPS mouse hearts. We showed that DNA damage accumulation led to the increase in CHK2 protein level, which enhanced the interaction between LKB1 and AMPKα, thereby promoting LKB1-mediated AMPKα phosphorylation and activating pro-atrophic signaling cascade. Importantly, we demonstrated that treatment of isoproterenol, an FDA-approved drug, could improve heart functions and extend the lifespan of HGPS mice.

Author contributions: Y.C., S.H., K.W., and Z.M. designed research; Y.C., S.H., Z. Cui, X.S., Y.T., H.Z., Z. Chen, R.J., W.Z., X.L., J.C., B.L., and Y.J. performed research; Y.C. and B.L. contributed new reagents/analytic tools; Y.C., S.H., H.Z., K.W., and Z.M. analyzed data; and Y.C., S.H., K.W., and Z.M. wrote the paper.

The authors declare no competing interest.

This article is a PNAS Direct Submission.

[1]Y.C. and S.H. contributed equally to this work.

[2]To whom correspondence may be addressed. Email: kewei@tongji.edu.cn or zhiyong_mao@tongji.edu.cn.

This article contains supporting information online at https://www.pnas.org/lookup/suppl/doi:10.1073/pnas.2309200120/-/DCSupplemental.

Published November 15, 2023.

introducing exogenous DNA into primary adult cardiomyocytes, it is necessary to create inducible-I-SceI mice that can be crossed with R26NHEJ mice. The resulting offspring can be used to measure changes in NHEJ efficiency in cardiomyocytes in vivo.

Adenosine monophosphate (AMP)-activated protein kinase (AMPK) functions as an energy sensor and comprises an α catalytic subunit along with regulatory β and γ subunits. It monitors the intracellular AMP: adenosine triphosphate ratio, ensuring a balance between anabolism and catabolism (14). While it is expected that cellular energy expenditure would be altered in response to genotoxic stress, the impact of DNA damage on AMPK activity remains unclear (14). Additionally, AMPK has been implicated in counteracting cardiac hypertrophy, and several AMPK activators have been utilized for this purpose (15). However, whether persistent activation of AMPK disrupts the cardiac homeostasis has not been extensively assessed.

In this study, we reported a cardiac atrophy phenotype, as well as an increasing amount of DSBs in the cardiomyocytes of a *Lmna*$^{G609G/G609G}$ (hereafter, HGPS) mouse model (5). Moreover, a transgenic mouse model was successfully established to provide direct evidence of NHEJ defects in the cardiomyocytes of HGPS mice. We subsequently dissected the molecular mechanism by which NHEJ deficiency led to the cardiac atrophy in HGPS cardiomyocytes through the CHK2-AMPKα-FOXO3A axis. In addition, through the utilization of isoproterenol (ISO), a U.S. Food and Drug Administration (FDA)-approved drug (16), we also identified possible intervention options that may be clinically utilized to treat HGPS patients.

Results

HGPS Mice Exhibit the Phenotype of Cardiac Atrophy. Cardiac aging is often accompanied with cardiac hypertrophy (17). To examine whether this outcome is present in HGPS cardiomyocytes, hearts were dissected from a previously reported HGPS mouse model (5). Contrary to our speculation, we observed smaller hearts, as determined by the ratio of heart weight to tibia length (HW/TL), in the 13- to 15-wk-old HGPS mice than in the age-matched wildtype (WT) mice (Fig. 1 *A* and *B* and *SI Appendix*, Fig. S1*A*). Hematoxylin and eosin (H&E) staining at the level of papillary muscle confirmed that the hearts of HGPS mice were obviously smaller than those of WT mice (Fig. 1*C*). However, the histological morphology of the heart and the extent of cardiac fibrosis, which was assessed by Masson's trichrome staining, showed no significant alterations (Fig. 1*C*). Immunostaining experiments with wheat germ agglutinin (WGA) (Fig. 1*D*) staining for cross-sectional area (CSA) analysis were also performed. Consistently, quantification of the cardiomyocyte CSA revealed that the cardiomyocyte size in the HGPS mice was actually significantly reduced, by ~20% (Fig. 1*E*). Adult cardiomyocytes were then isolated from WT and HGPS hearts, and measuring the cell size ex vivo further confirmed our observation (Fig. 1 *F* and *G*). Furthermore, our findings revealed a significant decrease in heart weight with increasing age in HGPS mice, whereas in WT mice, the heart weight gradually increased (Fig. 1*H*). We also found that the apoptotic rate was significantly increased in HGPS cardiomyocytes compared to that of WT cardiomyocytes (*SI Appendix*, Fig. S1 *B–D*). However, the increased apoptotic rate did not lead to a significant reduction in the number of cardiomyocytes in HGPS hearts (*SI Appendix*, Fig. S1*E*).

Furthermore, associated with the phenotype of cardiac atrophy, an echocardiographic (ECHO) analysis confirmed that parameters reflecting cardiac functions, including ejection fraction (EF) and fractional shortening (FS), were significantly reduced in HGPS mice, indicating deteriorated cardiac function (Fig. 1 *I* and *J* and *SI Appendix*, Fig. S1*F*). Data mining of previously published RNA-seq results obtained with HGPS and WT mouse hearts (7) revealed that a number of genes were differentially expressed between the two groups. Particularly, genes enriched in pathways that regulate cell growth and cell size were down-regulated, while genes in pathways regulating cellular responses to DNA damage, macromolecule catabolism, and the proapoptotic process, were up-regulated in HGPS hearts (Fig. 1 *K* and *L* and *SI Appendix*, Fig. S2). Notably, two major regulators facilitating protein degradation and muscle atrophy, namely, *Fbxo32* (also known as Atrogin-1) and *Trim63* (also known as MURF1) (18, 19), were both found to be significantly up-regulated in the hearts of the HGPS mice (*SI Appendix*, Fig. S2), consistent with the observed cardiac atrophy phenotype.

The In Vivo Reporter System Reveals Impaired NHEJ Capacity in HGPS Mouse Cardiomyocytes. The rise in genomic instability is the fundamental hallmark of premature aging and physiological aging, and accumulation of DSBs has been observed in both naturally aged and HGPS animals or humans (8, 20–23). To dissect the molecular mechanism underlying cardiac atrophy in HGPS mice, we sought to examine genomic stability in HGPS hearts. Genes involved in DNA damage response were found to be up-regulated in HGPS hearts (*SI Appendix*, Fig. S2), indicating an elevated level of DNA damage. To further support this finding, γH2AX, a marker of DSBs, was assessed in the hearts of HGPS mice. Both western blot analysis and immunofluorescence assays revealed that the amount of γH2AX was significantly increased in the hearts of HGPS mice compared to that of WT mice (Fig. 2 *A–D* and *SI Appendix*, Fig. S3*A*). Next, cardiomyocytes were isolated from the hearts of HGPS mice and WT mice for use in a comet assay. The results confirmed that genomic instability was increased by ~1.7-fold in HGPS cardiomyocytes (Fig. 2 *E* and *F*). Moreover, a similar result was obtained when genomic instability was measured by another well-accepted parameter, namely, the percentage of DNA in the tail (24) (*SI Appendix*, Fig. S3*B*).

While accumulating evidence suggests that deficiencies in DSB repair are closely related to aging in various organs, the role of DSB repair alterations in cardiomyopathy has not been extensively studied. Since the NHEJ pathway is active primarily during the G1 stage (26), which is the cell cycle phase where postmitotic adult cardiomyocytes are arrested, we hypothesized that Progerin impairs DSB repair via NHEJ, thereby destabilizing the genome in cardiomyocytes. In our previous studies, we developed an R26NHEJ reporter mouse with a GFP-based NHEJ reporter integrated at the *Rosa26* site for ex vivo NHEJ efficiency analysis (Fig. 2*G*) (13, 27). The I-SceI-encoding plasmid was transfected into primary cells isolated from R26NHEJ mice to generate a DSB in the reporter, and successful NHEJ reconstituted functional GFP. Although several protocols have been optimized, it is technically difficult to extract and maintain primary adult cardiomyocytes in vitro, and introducing exogenous DNA into primary cardiomyocytes is extremely inefficient via traditional approaches (28, 29). Thus, to test our aforementioned hypothesis, in vivo analysis tools need to be established for examining the change in NHEJ efficiency in HGPS hearts. We therefore created a transgenic mouse model, named, tg*Breaker*, that harbored a doxycycline-inducible I-SceI expression vector (Fig. 2*H*) (30, 31). We first characterized the tg*Breaker* mice by feeding them doxycycline-supplemented water for 9 consecutive days (*SI Appendix*, Fig. S4*A*). As expected, I-SceI expression was observed in several organs such as hearts (*SI Appendix*, Fig. S4 *B* and *C*). Given that previous studies have shown cell type–specific expression patterns in transgenic mice (32), we conducted further investigations to ascertain the specific cell types in which the expression of I-SceI is induced upon doxycycline treatment. Coimmunostaining experiments with

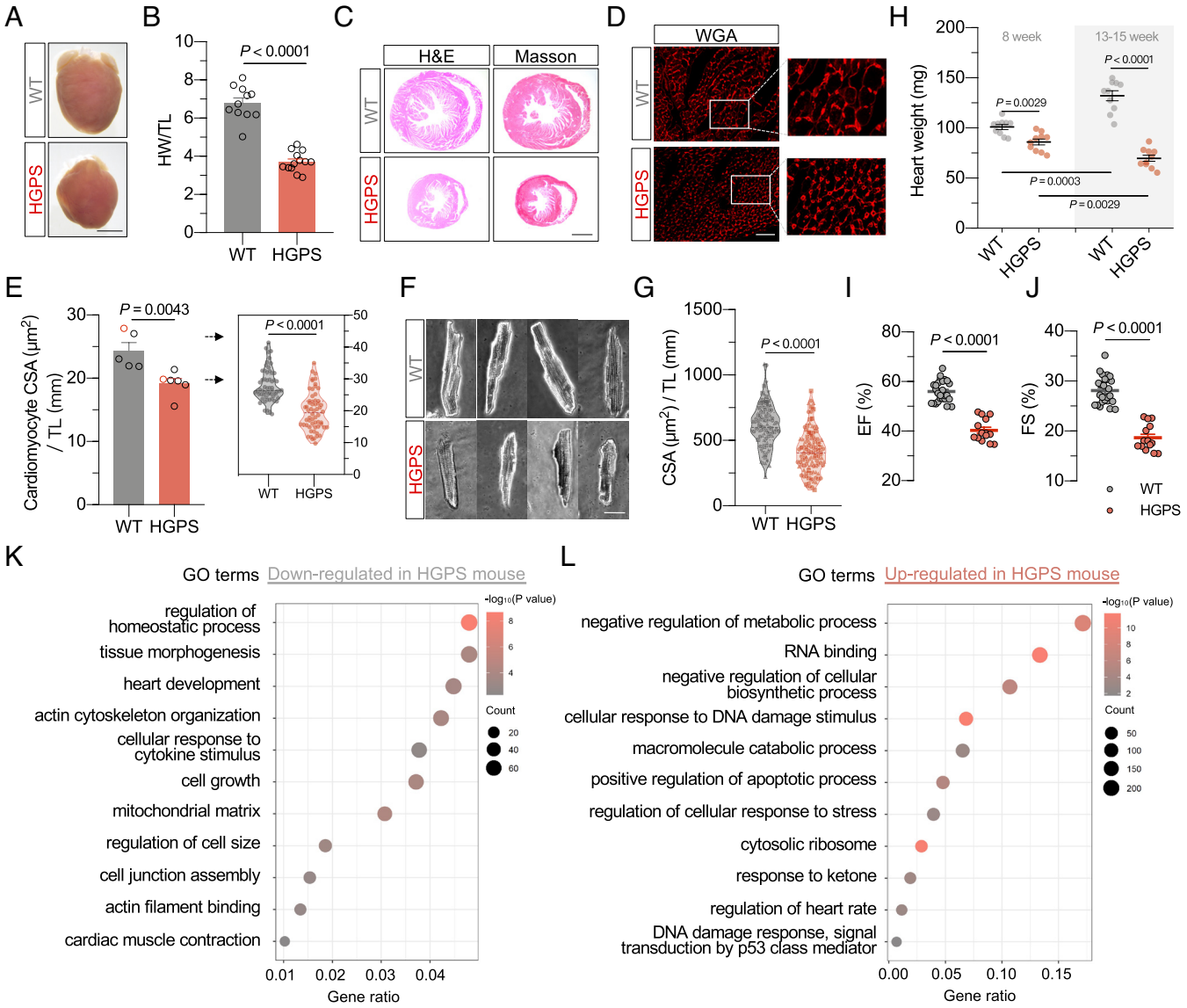

Fig. 1. HGPS mice exhibit the cardiac atrophy phenotype. (*A*) Hearts dissected from WT and HGPS mice. (Scale bar: 500 μm.) (*B*) Relative heart weight measured by the ratio of heart weight (mg) to tibia length (mm) (n > 5 mice per group). (*C*) H&E and Masson's trichrome staining of WT and HGPS hearts. (Scale bar: 500 μm.) (*D* and *E*) The cross-sectional area (CSA) of cardiomyocytes. Immunofluorescence staining of cardiac tissues with Alexa Fluor 594-WGA conjugate is shown in (*D*). (Scale bar: 200 μm.) Each dot represents one mouse in the left panel of (*E*) (WT, n = 5; HGPS, n = 6). The detailed cell size data for two representative mice, which are highlighted in red color, are shown in the right panel (each dot represents one cardiomyocyte). (*F* and *G*) Relative CSA of cardiomyocytes dissociated from WT and HGPS mice. (Scale bar: 50 μm.) The value was normalized to tibia length. (*H*) The heart weight of WT and HGPS mice at the indicated ages. (*I* and *J*) Analysis of cardiac function in 13- to 15-wk-old mice via echocardiography. Each dot represents one mouse. (*K* and *L*) Gene Ontology analysis based on the RNA-seq data [GSE124087 (7)] of WT and HGPS mouse hearts (n = 4). Mann–Whitney *U* test for (*B*, *E*, and *G*–*J*).

antibodies against HA (I-SceI) and the cardiomyocyte marker α-Actinin or the fibroblast marker Vimentin revealed that I-SceI was expressed in the nucleus of cardiomyocytes, and we observed that 35% of the cardiomyocytes analyzed expressed I-SceI (*SI Appendix*, Fig. S4 *D*–*G*). Confocal z-stack immunofluorescence labeling confirmed that I-SceI was specifically expressed in the nucleus of α-Actinin-positive cardiomyocytes (*SI Appendix*, Fig. S4*H*).

We then crossed the tg*Breaker* mice with R26NHEJ reporter mice and obtained *Rosa26*$^{NHEJ/+}$ tg*Breaker* mice. After 15 consecutive days of doxycycline administration, immunofluorescence experiments with antibodies against GFP and α-Actinin revealed that ~30% of the cardiomyocytes had successfully undergone DSB repair via NHEJ (*SI Appendix*, Fig. S4 *A*, *I*, and *J*). We then bred the *Rosa26*$^{NHEJ/+}$ mice with tg*Breaker* mice and *Lmna*$^{G609G/+}$ mice to obtain *Lmna*$^{G609G/G609G}$*Rosa26*$^{NHEJ/+}$ tg*Breaker* (HGPS *Rosa26*$^{NHEJ/+}$ tg*Breaker*) mice. After feeding the HGPS or control *Rosa26*$^{NHEJ/+}$tg*Breaker* mice doxycycline-supplemented water for 15 consecutive days, we killed the mice and harvested the hearts for analysis of NHEJ efficiency (Fig. 2*I*). We found that the percentage of GFP^{+} cardiomyocytes was significantly reduced, by ~50%, in the hearts of the HGPS mice (Fig. 2 *J* and *K*), indicating impaired NHEJ pathway in the cardiomyocytes. Moreover, we did not observe any difference in the transcript level of *Rosa26* (Fig. 2*L*) and the HA-I-SceI expression and cutting efficiency (Fig. 2*M* and *SI Appendix*, Fig. S4*K*) in HGPS and control *Rosa26*$^{NHEJ/+}$tg*Breaker* mice.

The Impaired Interaction of Progerin and γH2AX Attenuates the Recruitment of Mutant Lamin A to Damage Sites, Disrupting the NHEJ Signaling Cascade. Since Lamin A is an endogenous activator of SIRT6 (33), which is recruited to DSB sites to regulate NHEJ (34–36), we hypothesized that Lamin A, but not Progerin,

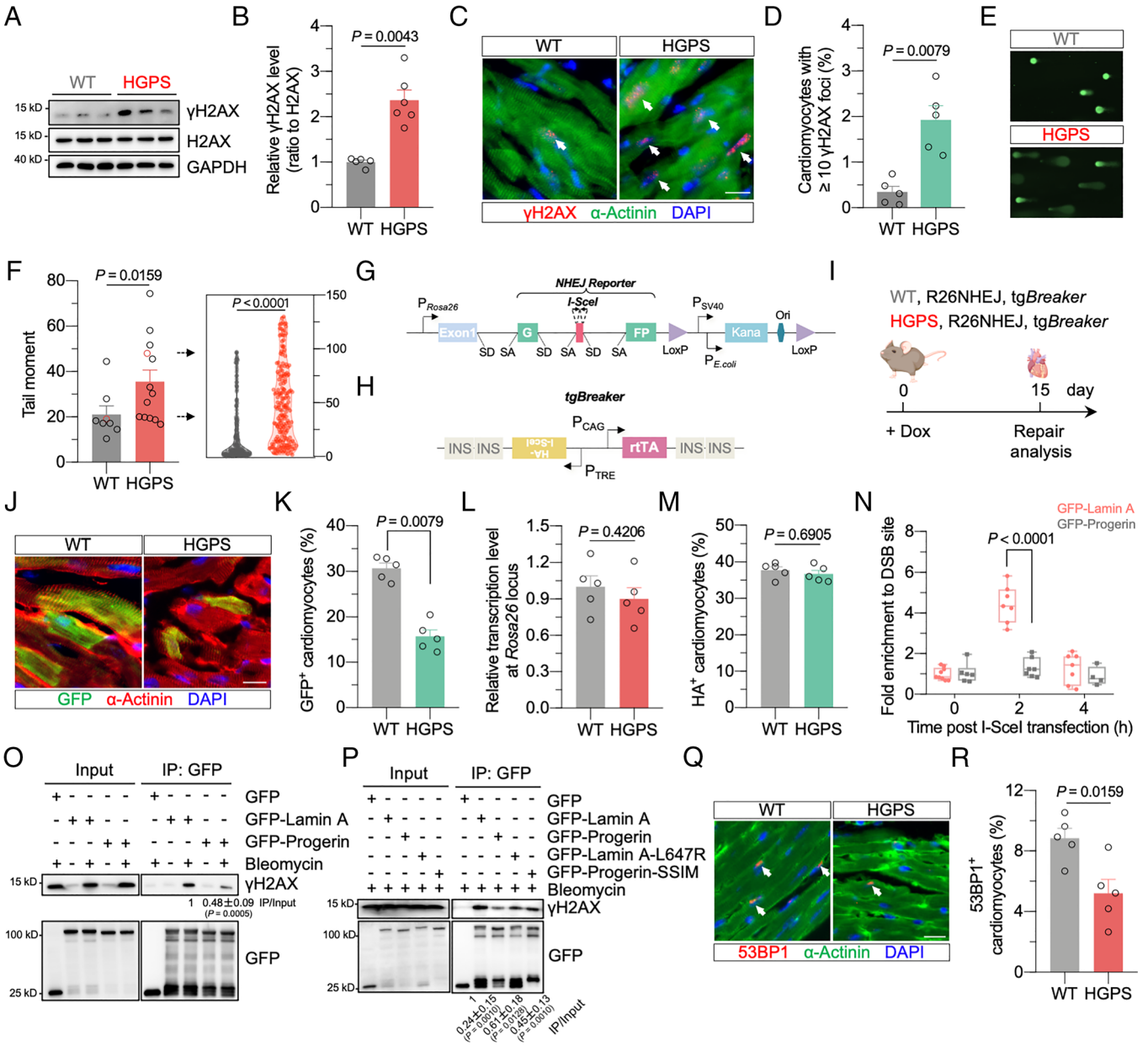

Fig. 2. Progerin-mediated NHEJ impairment contributes to genome instability in the cardiomyocytes of HGPS mice. (*A* and *B*) γH2AX levels in WT and HGPS hearts (WT, n = 5; HGPS, n = 6). (*C* and *D*) Analysis of the γH2AX level in the cardiomyocytes by coimmunostaining with antibodies against γH2AX and cardiomyocyte marker α-Actinin (Scale bar: 50 μm) (n = 5). (*E* and *F*) Analysis of genomic stability by comet assay (WT, n = 8; HGPS, n = 13). For the left panel in (*F*), each dot represents one mouse. The right panel shows the tail moment distribution for the mice highlighted in red in the left panel, and each dot represents one comet. (*G*) Schematic diagram showing the NHEJ reporter. (*H*) Schematic diagram showing the inducible I-SceI expression system for the construction of tg*Breaker* mice. (*I*) Experimental design for NHEJ efficiency analysis. (*J* and *K*) NHEJ efficiency of cardiomyocytes from 10- to 12-wk-old WT and HGPS mice (n = 5). (Scale bar: 50 μm.) (*L* and *M*) Transcription of the *Rosa26* locus and HA-I-SceI expression in the hearts of WT and HGPS mice fed doxycycline. (*N*) Chromatin immunoprecipitation (ChIP) assay showing the recruitment of Lamin A and Progerin to DSB sites in previously reported NHEJ-I9A reporter cell line (25). (*O*) Analysis of Lamin A/Progerin–γH2AX interaction in HEK293T cells. Cells were treated with or without 50 μM bleomycin for 2 h to induce DNA damage. (*P*) Analysis of the interaction between Lamin A mutants with γH2AX in HEK293T cells. (*Q* and *R*) Immunofluorescence analysis of 53BP1 in WT and HGPS hearts (n = 5). (Scale bar: 50 μm.) The error bars indicate the SEM values if not specifically indicated. Student's *t* test for (*N*–*P*), and Mann–Whitney *U* test for other panels.

is recruited to DSB sites to activate the subsequent NHEJ signaling cascade. Using our NHEJ-I9A reporter cell line (25, 37–39), we found that Lamin A, but not Progerin, was recruited to the I-SceI-generated DSB sites (Fig. 2*N*). The formation of γH2AX at DSB sites is suggested to serve as docking sites for DSB damage response proteins such as 53BP1 (40, 41); therefore, we sought to determine whether the failed recruitment of Progerin to DSB sites is due to the diminished interaction between Progerin and γH2AX. Indeed, we observed that Lamin A interacted with γH2AX, while Progerin showed a markedly diminished interaction with γH2AX after DNA damage was induced in HEK293T cells and NRVCs (Fig. 2*O* and *SI Appendix*, Fig. S5*A*). Furthermore, co-IP experiments using two previously reported Lamin A mutants, permanently farnesylated Lamin A-L647R (42) and unfarnesylated Progerin-SSIM (43), indicated that both the presence of farnesylation and the loss of 50 amino acids in Progerin contributed to the decrease in the interaction between γH2AX and Progerin (Fig. 2*P*). Moreover, consistent with previous reports (8, 9), immunofluorescence experiments indicated that, although the number of DSBs in HGPS cardiomyocytes was much higher than that in WT mice (Fig. 2 *A*–*D*), the number of 53BP1 foci was significantly reduced in the cardiomyocytes of HGPS mice

(Fig. 2 *Q* and *R* and *SI Appendix*, Fig. S5*B*). These results indicate that the structural alteration of Progerin diminished its interaction with γH2AX, thereby suppressing the recruitment of Progerin to DSB sites and abolishing the subsequent recruitment of critical DNA damage response proteins such as 53BP1.

DNA Damage Checkpoint Regulator CHK2 Interacts with AMPKα. It is predictable that the decline in NHEJ destabilizes the genome, thereby promoting the apoptosis of cardiomyocytes (44, 45). However, whether the NHEJ decline-mediated increase in genome instability causes cardiac atrophy in HGPS mice remained to be determined. Previous studies have demonstrated that unrepaired DSBs might cause a persistent DNA damage response, which is mainly mediated via ATM and CHK2 in G1 phase-arrested cells (46). In the present study, a western blot analysis indicated that both the phosphorylation levels of ATM and CHK2, as well as the protein level of CHK2, were increased in HGPS mouse hearts (Fig. 3 *A* and *B* and *SI Appendix*, Fig. S6 *A* and *B*). The increased CHK2 protein level was not due to the upregulation of CHK2 mRNA expression (*SI Appendix*, Fig. S6*C*), indicating that, consistent with previous reports (47, 48), CHK2 might be regulated at the posttranslational level. AMPKα is the key protein regulating the size of muscle cells and the hypertrophic growth of the heart (49), and its activation is dependent on the phosphorylation at the Thr172 site within the catalytic domain (50). A western blot analysis revealed that the phosphorylation level of AMPKα was significantly increased in the hearts of the HGPS mice (Fig. 3 *C* and *D*). Immunofluorescence experiments were also performed to confirm our finding (Fig. 3 *E* and *F*). Since AMPKα activity was reduced by overactivated DNA-PKcs

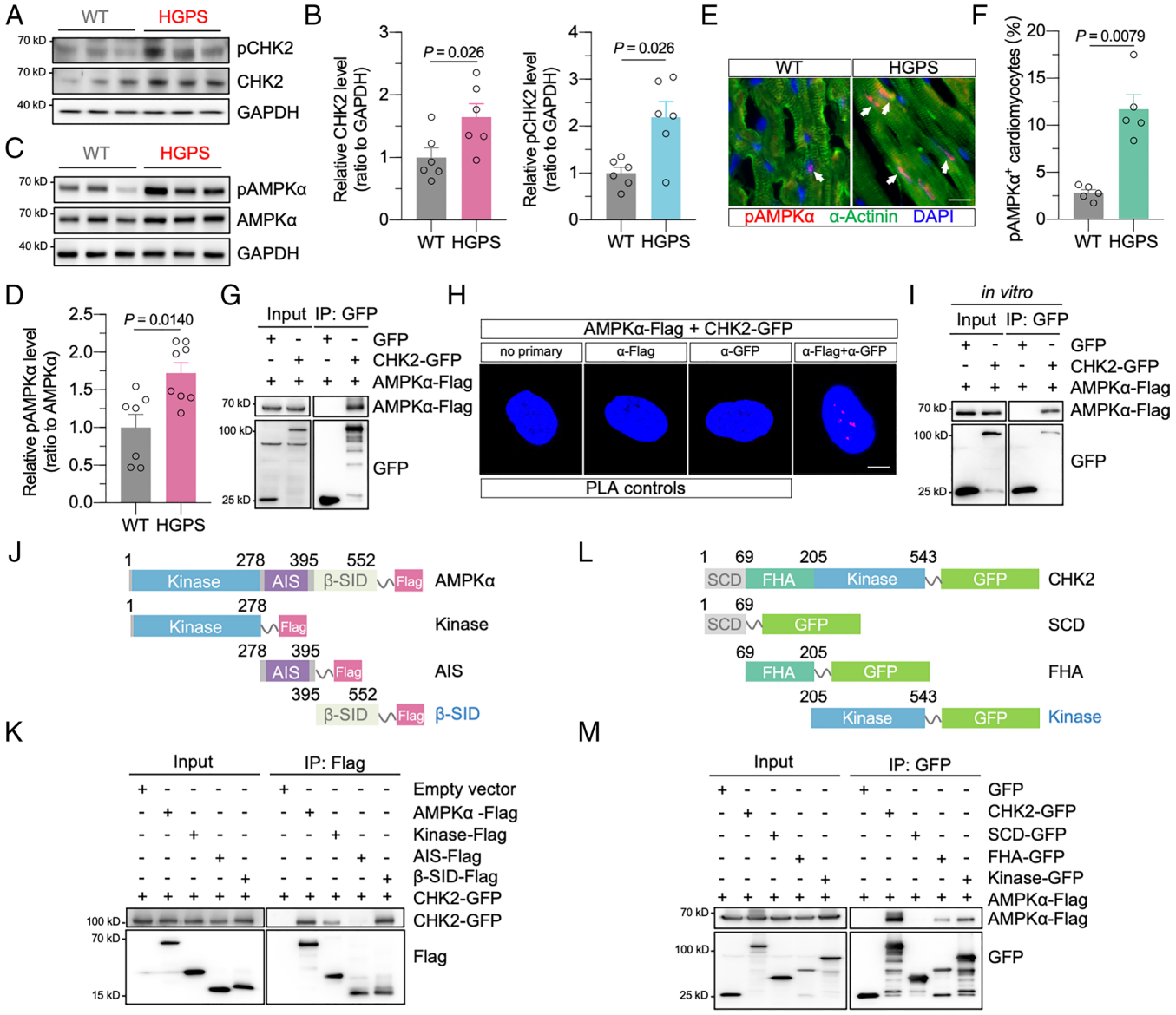

Fig. 3. CHK2 interacts with AMPKα. (*A* and *B*) Protein levels of phosphorylated CHK2 (pCHK2) (Thr68) and CHK2 in WT and HGPS hearts (n = 6 mice). (*C* and *D*) Protein levels of phosphorylated AMPKα (pAMPKα) (Thr172/183) in WT and HGPS hearts (WT, n = 7; HGPS, n = 8). (*E* and *F*) Analysis of the pAMPKα level in the cardiomyocytes of WT and HGPS mice (n = 5 mice). (Scale bar: 50 μm.) (*G*) Protein interaction between CHK2 and AMPKα in HEK293T cells. Cells transfected with the indicated vectors were harvested for co-IP with an antibody against GFP. (*H*) Validation of the protein interaction between CHK2 and AMPKα with an in situ PLA assay. (Scale bar: 5 μm.) (*I*) Analysis of the CHK2-AMPKα interaction with an in vitro pull-down assay. (*J*) Schematic representation of Flag-tagged full-length and truncated AMPKα. (*K*) Identification of the domains in AMPKα that mediate its interaction with CHK2. (*L*) Schematic representation showing GFP-tagged full-length and truncated CHK2. (*M*) Identification of the domains in CHK2 that mediate its interaction with AMPKα. All experiments were repeated at least three times. The error bars indicate the SEM values. Mann–Whitney *U* test for (*B*, *D*, and *F*).

in aged skeletal muscle (51), we performed a western blot analysis with antibodies against DNA-PKcs and its phosphorylated form. We ruled out the possibility that the alteration of AMPKα phosphorylation was mediated by DNA-PKcs, as its expression and phosphorylation were not significantly changed in the hearts of HGPS mice (*SI Appendix*, Fig. S6 *D* and *E*). Several possible reasons might explain the difference in DNA-PKcs activation between the HGPS and normally aged mice. First, in comparison to normal cells, HGPS vascular smooth muscle cells and fibroblasts showed decreased nuclear distribution of DNA-PKcs (52). Second, reduced 53BP1 recruitment to DNA damage sites in HGPS cells might impair the transduction of the NHEJ signaling cascade, which may have resulted in the unsuccessful activation of DNA-PKcs. Finally, the differences may be tissue specific.

Since both ATM and CHK2 are activated in HGPS hearts, we hypothesized that the upregulation of AMPKα phosphorylation levels was mediated by ATM and/or CHK2. Co-IP experiments demonstrated that AMPKα interacted with CHK2, but no obvious interaction between ATM and AMPKα was observed (Fig. 3*G* and *SI Appendix*, Fig. S6 *F* and *G*), suggesting that AMPKα might be a substrate of the CHK2 kinase. To test this possibility, subcellular fractionation with HEK293T cells and co-IP experiments with the cytosol and nuclear fractions were performed, and our results showed that CHK2 and AMPKα interacted mainly in the nucleus (*SI Appendix*, Fig. S6*H*). A proximity ligation assay (PLA) confirmed the interaction between CHK2 and AMPKα in the nucleus (Fig. 3*H*). Moreover, using purified recombinant proteins, the interaction between CHK2 and AMPKα was observed in vitro (Fig. 3*I*). Then, we set out to determine which domains in AMPKα interacted with CHK2. Vectors encoding different domains of AMPKα and CHK2 were created on the basis of previous studies (53, 54). By performing co-IP experiments with vectors expressing full-length and truncated AMPKα or CHK2, we found that both the kinase domain and β-SID domain of AMPKα interacted with CHK2 (Fig. 3 *J* and *K*). Co-IP experiments also revealed that the FHA and kinase domains of CHK2 interacted with AMPKα (Fig. 3 *L* and *M*).

CHK2 Promotes the LKB1-AMPKα Interaction to Activate AMPKα and FOXO3A-Mediated Pro-Atrophic Signaling. Because CHK2 is a kinase, we first speculated that the CHK2-AMPKα interaction contributes to the CHK2-mediated phosphorylation and activation of AMPKα. As expected, we found that CHK2 overexpression promoted AMPKα phosphorylation (Fig. 4*A*), and knocking down CHK2 abolished the stress-dependent upregulation of AMPKα phosphorylation (Fig. 4*B* and *SI Appendix*, Fig. S7*A*). However, the enzymatically dead CHK2 mutant CHK2-D347A (55) interacted with AMPKα (*SI Appendix*, Fig. S7*B*), and retained the stimulatory effect on AMPKα phosphorylation (Fig. 4*C*). Consistently, inhibiting the CHK2 kinase with its inhibitor BML-277 (56) did not abolish the stress-dependent phosphorylation of AMPKα (Fig. 4*D*). These results indicate that the stimulation of AMPKα phosphorylation by CHK2 was independent of its enzymatic activity. Since AMPKα is the substrate of LKB1 (57), we hypothesized that CHK2 might promote the LKB1-AMPKα interaction to facilitate the subsequent phosphorylation of AMPKα by LKB1. Co-IP experiments revealed that CHK2 interacted with LKB1 (Fig. 4*E* and *SI Appendix*, Fig. S7*C*), and the interaction was mediated by the FHA and kinase domains of CHK2 (*SI Appendix*, Fig. S7*D*). Moreover, CHK2 overexpression greatly enhanced the LKB1-AMPKα interaction (Fig. 4*F* and *SI Appendix*, Fig. S7*E*), while depleting CHK2 expression attenuated the LKB1-AMPKα interaction (Fig. 4*G* and *SI Appendix*, Fig. S7*F*). Thus, we hypothesized that CHK2 acts as a scaffold to improve LKB1-AMPKα interaction. Consistently, deleting FHA and kinase domains (SCD-GFP) abolished the stimulatory effect of CHK2 on LKB1-AMPKα interaction (Fig. 4*H*).

Previous studies have shown that AMPKα phosphorylates the atrophy-related transcription factor Forkhead BoxO3 (FOXO3A) (58) at the Ser 413 residue, resulting in its activation. Additionally, AMPKα inhibits the mTOR signaling pathway to delay anabolic processes (59). As expected, we observed an increase in the phosphorylation level of FOXO3A in the hearts of HGPS mice (Fig. 4 *I* and *J* and *SI Appendix*, Fig. S7*G*). We also examined the phosphorylation levels of 4EBP1 and S6K1, two critical downstream signaling factors of the mTOR pathway. The results showed that phosphorylation of 4EBP1 was down-regulated, but there was no obvious change in S6K1 phosphorylation in the hearts of the HGPS mice (*SI Appendix*, Fig. S7 *H–K*). FOXO3A has been reported to activate the transcription of several cardiac and skeletal muscle-specific atrophy-related ubiquitin ligases, such as Atrogin-1 (*Fbxo32*) and MURF1 (*Trim63*) (18, 19). Therefore, real-time quantitative PCR was performed, and the results clearly demonstrated that the mRNA levels of both factors were significantly elevated in the HGPS hearts (Fig. 4 *K* and *L*), consistent with the RNA-seq data (*SI Appendix*, Fig. S2). To validate our findings in vitro, primary NRVCs were subjected to X-rays, and AMPKα phosphorylation and atrogene expression were then analyzed. The immunostaining results analyzed with a high-content imaging system revealed that AMPKα phosphorylation was significantly elevated after the X-ray treatment (Fig. 4 *M* and *N* and *SI Appendix*, Fig. S7 *L* and *M*), and the transcription of *Fbxo32* and *Trim63* was activated (Fig. 4 *O* and *P*). To further validate our findings, NRVCs transfected with siRNA against CHK2 or control siRNA were irradiated, and RT-qPCR analysis confirmed that both the transcription of *Fbxo32* and *Trim63* were significantly decreased in CHK2 knockdown NRVCs compared to control cells (Fig. 4 *Q–S*). Moreover, depletion of CHK2 significantly increased the cardiomyocyte size measured by the area of individual NRVCs (Fig. 4 *T* and *U*). Together, these data demonstrate that the DNA damage-induced increase in the CHK2 protein level promotes LKB1-mediated AMPKα phosphorylation to activate FOXO3A, resulting in elevated cardiac atrophy programs.

Targeted Inhibition of AMPK Activity Enlarges the Heart of HGPS Mice. To further demonstrate that the phenotype of cardiac atrophy is mediated by the activity of AMPKα, NRVCs were treated with the AMPK inhibitor, Compound C (CC) (60–62), then stained with anti-pAMPKα or/and anti-α-Actinin, and analyzed on a high-content imaging system. CC treatment significantly decreased the level of phosphorylated AMPKα (Fig. 5 *A* and *B*) and increased the cell size of NRVCs (Fig. 5 *C* and *D*). To investigate the efficacy of CC treatment in vivo, HGPS mice were injected intraperitoneally with CC (10 mg/kg) for four times with a 3-d interval between each injection (Fig. 5*E*). Consistently, CC significantly enlarged the heart, as well as the size of the cardiomyocytes (Fig. 5 *F–H*) of HGPS mice. In addition, the phosphorylation of both AMPKα and FOXO3A (Fig. 5 *I–L*) was greatly attenuated after CC injection, indicating that the AMPK-mediated atrophy-promoting signaling was inhibited. Collectively, our data demonstrated that targeting AMPK could significantly ameliorated the cardiac atrophic phenotype both in vitro and in vivo.

Forced Enlargement of Cardiomyocytes to a Normal Size Reestablishes Cardiac Function and Extends the Lifespan of HGPS Mice. AMPK is a master regulator of the whole-body energy balance, thus directly targeted inhibition of AMPK with CC might influence the energy homeostasis of multiple organs and not be a suitable clinical approach. Therefore, we set out to look

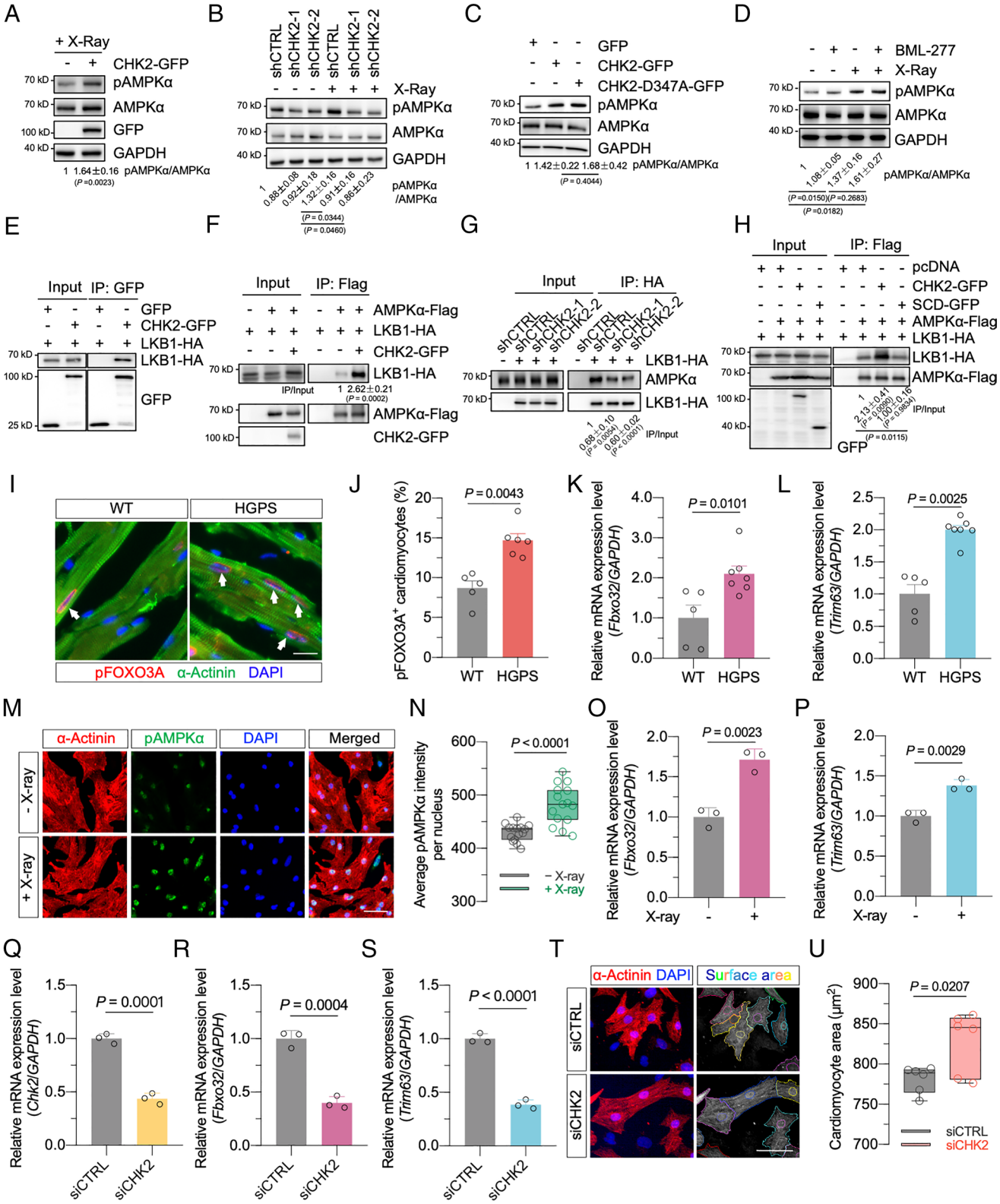

Fig. 4. CHK2 activates AMPKα by enhancing its interaction with LKB1. (*A*) CHK2 overexpression on AMPKα phosphorylation level after exposure to 10 Gy ionizing radiation (IR). (*B*) The effect of CHK2 depletion on AMPKα phosphorylation post IR. (*C*) The effect of overexpressing WT or enzymatically dead CHK2 on AMPKα phosphorylation post IR. (*D*) The effect of treatment with 10 μM CHK2 inhibitor BML-277 on AMPKα phosphorylation. (*E*) Analysis of CHK2-LKB1 interaction in HEK293T cells. (*F*) The effect of CHK2 overexpression on the AMPKα-LKB1 interaction. (*G*) Analysis of AMPKα-LKB1 interaction in CHK2-knockdown HEK293T cells. (*H*) The effect of overexpressing full-length or truncated CHK2 on the AMPKα-LKB1 interaction. (*I* and *J*) Immunofluorescence staining of phosphorylated FOXO3A in heart sections (WT, n = 5; HGPS, n = 6). (Scale bar: 50 μm.) (*K* and *L*) Analysis of the mRNA levels of *Fbxo32* (*K*) and *Trim63* (*L*) in the hearts (WT, n = 5; HGPS, n = 7). (*M* and *N*) Analysis of pAMPKα intensity in NRVCs at 15 min post 10 Gy IR. The intensity of the pAMPKα signal was analyzed on a high-content imaging platform. Each dot represents the average pAMPKα signal intensity per cardiomyocyte nucleus per well. (Scale bar: 50 μm.) (*O* and *P*) Analysis of the mRNA levels of *Fbxo32* (*O*) and *Trim63* (*P*) in NRVCs at 48 h post 10 Gy IR. (*Q*–*S*) Analysis of the mRNA levels of *Chk2* (*Q*), *Fbxo32* (*R*), and *Trim63* (*S*) in NRVCs transfected with siRNA against CHK2 or control siRNA at 24 h post 10 Gy IR. (*T* and *U*) Analysis of the cell sizes of NRVCs transfected with siRNA against CHK2 or control siRNA on a high-content imaging platform. (Scale bar: 50 μm.) The error bars indicate the SEM values in (*J*–*L*) and the SD values in (*O*–*S*). Mann–Whitney *U* test for (*J*–*L*) and Student's *t* test for other panels.

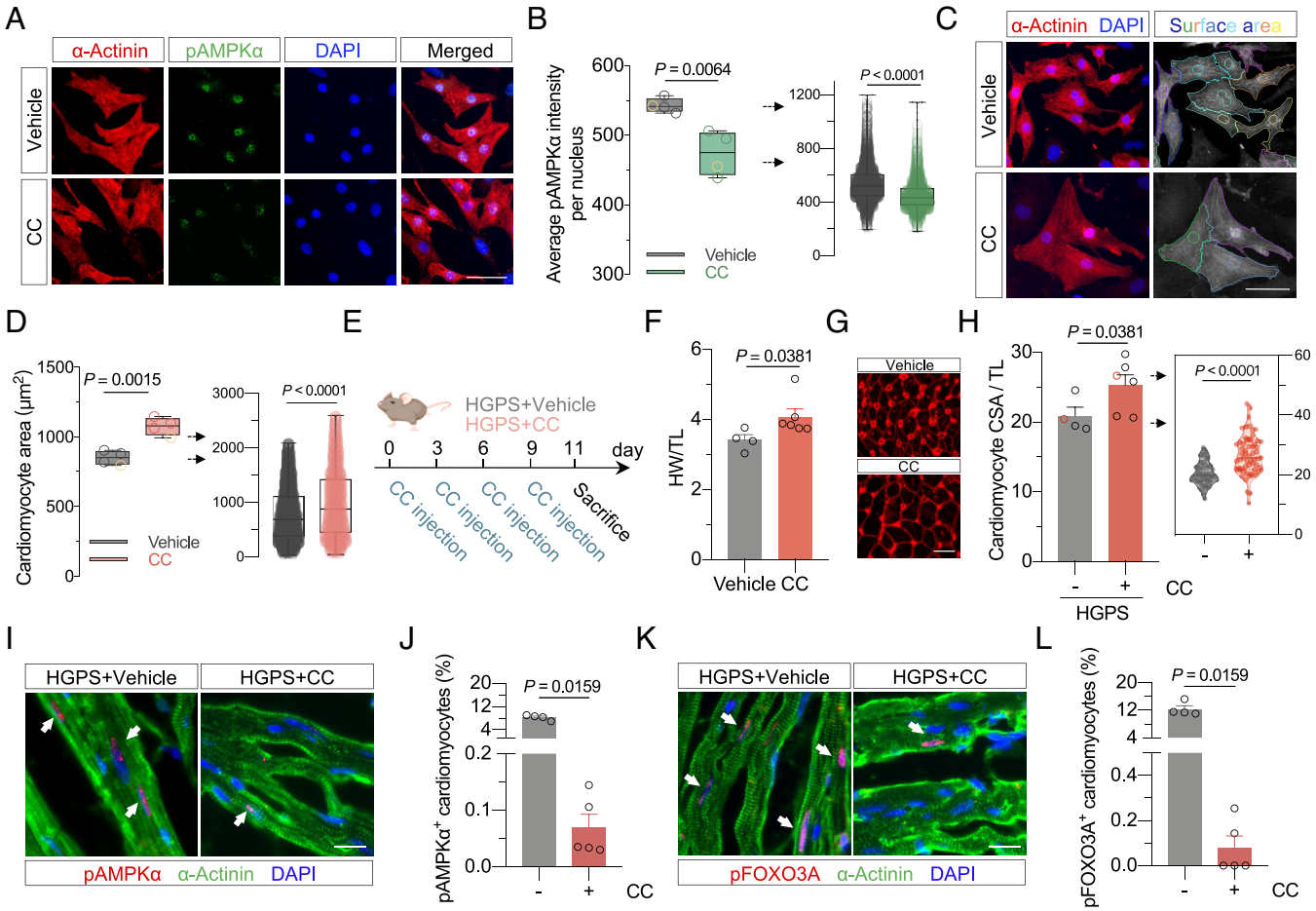

Fig. 5. Inhibiting AMPK activity enlarges cardiomyocytes in vitro and in vivo. (*A* and *B*) Analysis of pAMPKα intensity in NRVCs. Cells were treated with 10 μM CC for 12 h and harvested for imaging at 24 h post CC withdrawal. (Scale bar: 50 μm.) Each dot represents the average intensity of the pAMPKα signal per cardiomyocyte nucleus in one well in the left panel of (*B*), and the pAMPKα signals for each cell are shown in the right panel. (*C* and *D*) Analysis of the cell sizes of NRVCs treated with or without CC. Cells were harvested for imaging at 72 h post CC withdrawal. (Scale bar: 50 μm.) (*E*) Experimental design for the CC treatment on HGPS mice. (*F*) Relative heart weight in HGPS mice with CC treatment (Vehicle, n = 4; CC, n = 6). (*G* and *H*) The CSA of cardiomyocytes in HGPS mice with CC treatment (Vehicle, n = 4; CC, n = 6). (*I* and *J*) Effect of CC treatment on pAMPKα level in HGPS cardiomyocytes (Vehicle, n = 4; CC, n = 5). (Scale bar: 50 μm.) (*K* and *L*) Effect of CC treatment on pFOXO3A level in HGPS cardiomyocytes (Vehicle, n = 4; CC, n = 5). (Scale bar: 50 μm.) The error bars indicate the SEM values. Student's *t* test for (*B* and *D*), and Mann–Whitney *U* test for (*F*, *H*, *J*, and *L*).

for clinically approved methods that can be employed to induce hypertrophic cardiomyocyte growth and to investigate whether cardiac atrophy, as well as decreased cardiac function and lifespan, in HGPS mice can be rescued. Isoproterenol (ISO), a β-adrenergic agonist, is a common stimulus for cardiac hypertrophy in vitro and in vivo and has been widely used in the clinic to treat heart block and bradycardia (16). Moreover, a previous study showed that ISO inactivated AMPKα in cardiomyocytes (63). Consistent with this, we confirmed that ISO treatment significantly reduced the phosphorylation of AMPKα in NRVCs (*SI Appendix*, Fig. S8 *A* and *B*), and increased the size of cardiomyocytes (*SI Appendix*, Fig. S8 *C* and *D*).

Therefore, we explored the efficacy of ISO treatment in attenuating cardiac atrophy in HGPS mice in vivo. Mice that were 8 to 9 wk old were injected with ISO twice for 7 consecutive days each time with a 14-d interval between the two treatment periods. ECHO was performed on the mice before the ISO injection and on Day 7 after the second period of ISO injection. The mice receiving ISO treatment were also analyzed by immunostaining and for ascertaining heart weight and lifespan (Fig. 6*A*). The hearts of the ISO-treated HGPS mice were enlarged, as measured by the ratio of the heart weight to the tibia length, compared to those in the control group (Fig. 6 *B* and *C*). H&E staining further indicated that the heart was obviously enlarged following ISO treatment, while cardiac fibrosis was not impacted (Fig. 6*D* and *SI Appendix*, Fig. S8*E*). We also found that ISO treatment significantly increased the size of the cardiomyocytes in both the WT and HGPS mice (Fig. 6 *E* and *F*). Notably, treatment with ISO resulted in the restoration of the heart size in HGPS mice to a normal level, comparable to the size of untreated WT hearts, and it did not induce hypertrophy (Fig. 6 *B* and *F*).

Mechanistically, the phosphorylation of both AMPKα (Fig. 6 *G* and *H*) and FOXO3A (Fig. 6 *I* and *J*) was reduced in the HGPS hearts following ISO injection, accompanied by a significant decrease in *Fbxo32* and *Trim63* transcription (*SI Appendix*, Fig. S8 *F* and *G*), indicating that atrophy-promoting signaling was blocked. However, we did not observe significant changes in the level of γH2AX (*SI Appendix*, Fig. S8 *H* and *I*) or the percentage of apoptotic cells (*SI Appendix*, Fig. S8 *J* and *K*). Since epigenetic alterations are one of the drivers of aging (64), and they have been reported to be associated with HGPS (65–67), we further tested whether ISO treatment affects epigenetics. However, ISO treatment did not result in any significant alterations in the dysregulated epigenetic modifications (*SI Appendix*, Fig. S8 *L* and *M*).

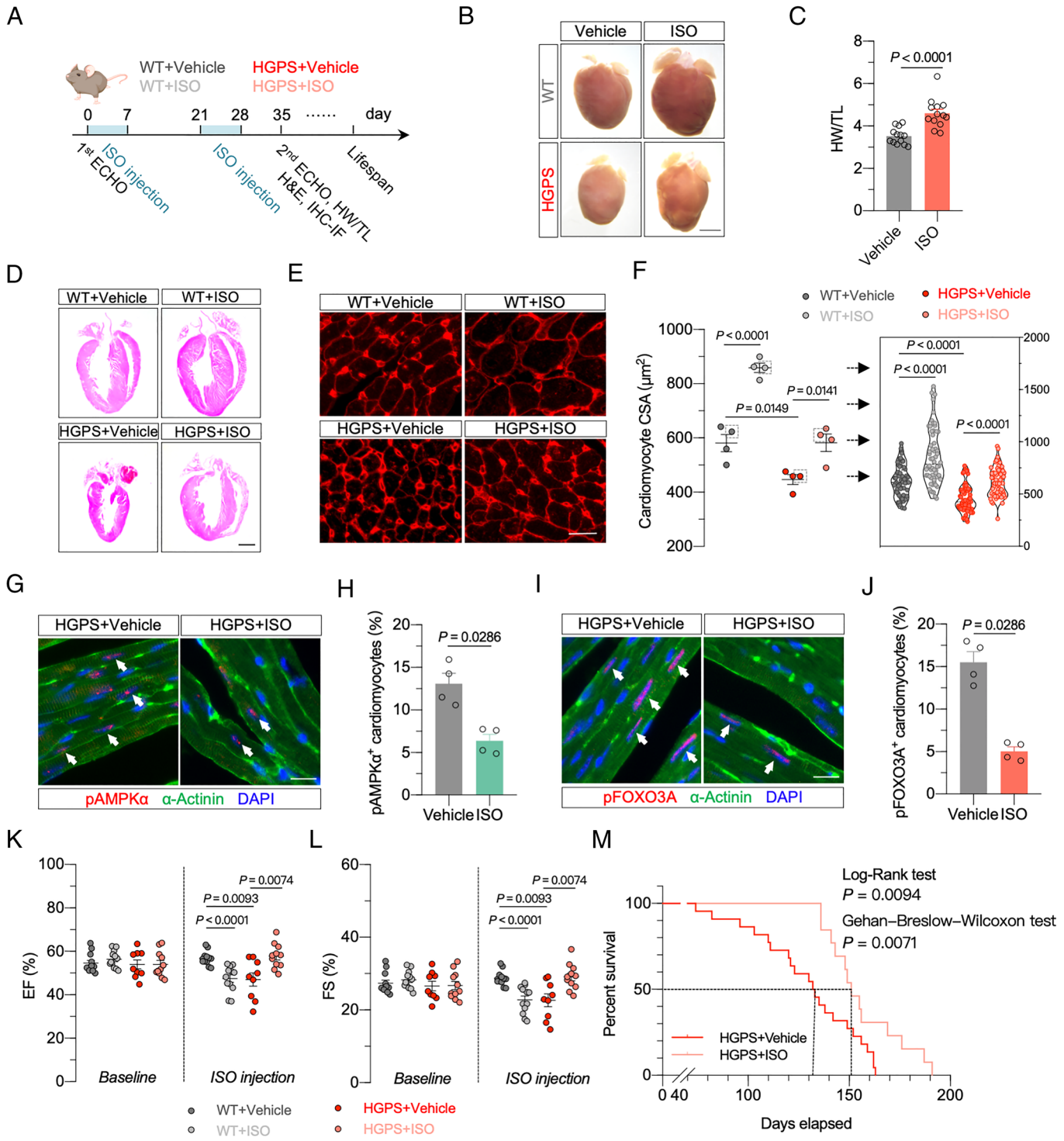

Fig. 6. Isoproterenol-induced enlargement of cardiomyocytes ameliorates cardiac dysfunction and extends the lifespan of HGPS mice. (*A*) Experimental design of ISO treatment experiment. (*B*) WT and HGPS heart with ISO injection. (Scale bar: 500 μm.) (*C*) The effect of ISO treatment on the relative heart weight of HGPS mice (n = 13 mice). (*D*) H&E staining of WT and HGPS hearts with ISO injection. (Scale bar: 500 μm.) (*E* and *F*) CSA of cardiomyocytes in WT and HGPS mice with ISO injection. (Scale bar: 50 μm.) Each dot represents one mouse in the left panel of (*F*) (n = 4 mice). For the mice highlighted with dashed-line boxes, detailed cell size data are shown in the right panel. (*G–J*) Effect of ISO treatment on pAMPKα level and pFOXO3A level in HGPS heart (n = 4 mice). (Scale bar: 50 μm.) The error bars indicate the SEM values. (*K* and *L*) Effect of ISO treatment on EF and FS. Notably, cardiac function followed a time-dependent decline in vehicle-treated HGPS mice while the decline was rescued by ISO treatment (n > 9 mice per group). The error bars indicate the SEM values. (*M*) Lifespan analysis of HGPS mice with (n = 13) or without (n = 22) ISO treatment. Mann–Whitney *U* test for (*C*, *H*, *J–L*), and one-way ANOVA for (*F*).

Our results imply that 1) ISO can be used to forcibly induce the hypertrophic growth of cardiomyocytes in HGPS mice, by possibly targeting the AMPKα-FOXO3A axis, and that 2) cardiac atrophy signaling is downstream of accumulated damaged DNA.

To investigate whether ISO-mediated rescue of the atrophy phenotype improves cardiac function, an ECHO analysis was carried out. The results revealed that treating mice with ISO significantly improved the heart function of HGPS mice but that ISO

treatment reduced the heart functions of the WT mice, consistent with previous studies (68) (Fig. 6 *K* and *L* and *SI Appendix*, Fig. S8*N*). These intriguing findings suggest that ISO administration exerts opposite effects on the heart function of WT mice and HGPS mice, which present with atrophied cardiac tissue. Moreover, ISO treatment mitigated the weight loss associated with HGPS (*SI Appendix*, Fig. S8*O*). Most importantly, treating HGPS mice with ISO significantly prolonged their mean lifespan, by 20.8% (from 130 d to 157 d), and the maximum lifespan was also increased by 17.2% (from 163 d to 191 d) (Fig. 6*M*), while no significant changes in the lifespan of WT mice treated with ISO were observed in a timeframe of 200 d (*SI Appendix*, Fig. S8*P*). Notably, ISO indeed increased load and stress to a normal heart, causing hypertrophy, and is overall deleterious to cardiac function, as shown in our results (Fig. 6 *B*, *K*, and *L*). However, as the major defect in the heart of the HGPS mouse is the rare cardiac atrophy, ISO may serve as a protective treatment against atrophic defect with a great translational promise. Collectively, our results suggest that forcible enlargement of cardiomyocytes in atrophic HGPS hearts to a normal size ameliorated heart function and extended the lifespan of the HGPS mice (Fig. 7).

Discussion

Cardiac abnormalities are closely associated with the mortality of HGPS patients (69). However, the impact of deficient DSB repair on cardiac abnormalities in HGPS has not been investigated. In our study, we utilized a mouse model, tg*Breaker*, in combination with previously described R26NHEJ mice to demonstrate that NHEJ is impaired in the hearts of HGPS mice. Consequently, the accumulation of unrepaired DSBs triggered the upregulation of CHK2 (47, 48), which promoted LKB1-AMPKα interaction as a scaffold, leading to sustained activation of the AMPKα signaling cascade and subsequent cardiac atrophy. Notably, AMPKα has been previously proven to counteract cardiac hypertrophy, and our findings underscore the significance of finely regulating AMPKα activity for maintaining cardiac homeostasis.

Consistent with our study, mice with deficiency in NHEJ exhibited cardiomyopathies (70, 71). Moreover, a number of chemotherapeutic agents that function by inducing DNA damage, such as doxorubicin, have also been reported to cause cardiac atrophy in both patients and animal models (72–75). The mechanistic link between DNA damage response and the cardiomyopathy we identified might help explain the age-related changes in the heart in both animal models and humans. However, whether other damage response factors play important roles in these processes warrants further investigation.

Although the discovery of effective therapies for HGPS remains extremely limited, numerous efforts have been dedicated to developing treatments for this syndrome. One potential approach involves inhibiting the isoprenylation of mutant Lamin A. Lonafarnib, a farnesyltransferase inhibitor (FTI) (76), became the first FDA-approved drug for HGPS treatment in the clinic in 2020 (77). However, long-term treatment with FTIs may lead to the accumulation of nonfarnesylated prelamin A, which has been linked to lethal cardiomyopathy in mouse models (78). Moreover, treating HGPS cells with metformin alleviates senescence phenotypes in vitro (79, 80). Intriguingly, AMPK signaling has been identified as a pharmacological target of metformin, and several studies have reported that metformin administration improved cardiac function in normal individuals (81). Nevertheless, it remains unclear whether AMPK activation by metformin benefits

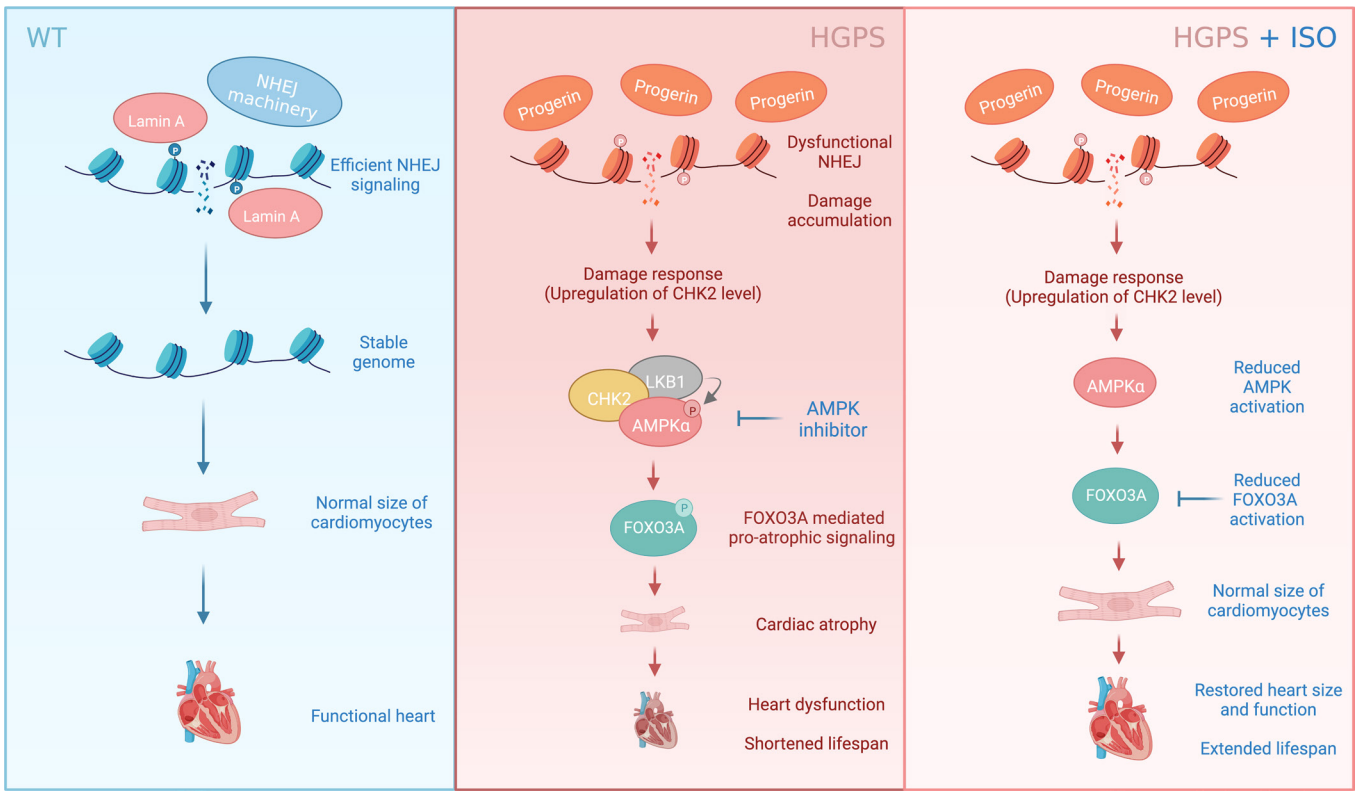

Fig. 7. Genome instability-induced cardiomyopathy in HGPS mice and the potential intervening approaches. Lamin A can be recruited to DSB sites to facilitate NHEJ repair. In HGPS mice, impaired Progerin recruitment disrupts downstream repair processes, resulting in DNA damage accumulation and increased CHK2 expression. CHK2 promotes AMPKα-LKB1 interaction, leading to AMPKα phosphorylation and activating FOXO3A-mediated atrophy-promoting signaling, contributing to decreased cell size. Inhibiting AMPK activity increases cardiomyocyte and heart size. Treating HGPS mice with ISO attenuated cardiac atrophy by suppressing AMPKα and FOXO3A phosphorylation and contributed to improved heart function and an extended lifespan.

the function of HGPS cardiac muscle cells, which already display hyperactive AMPK signaling, or whether it can prolong the survival of HGPS individuals.

Importantly, we unexpectedly found that ISO treatment enhanced heart function and increased the lifespan of HGPS mice. Fortunately, ISO has been approved for clinical use for a considerable period, which opens up promising possibilities for utilizing ISO as a standalone treatment or in combination with other drugs targeting additional symptoms associated with HGPS, in order to achieve improved treatment outcomes. However, further research is necessary to determine the effectiveness and optimal treatment regimen of ISO in mice and other animal models, as well as in HGPS patient-induced pluripotent stem cell-derived cardiomyocytes, before the safe and effective translation to the benefit of patients. Furthermore, investigating the potential of directly activating the NHEJ pathway to alleviate cardiomyopathy and extend lifespan represents an additional valuable avenue for investigation.

Materials and Methods

A detailed description of the materials and methods used for this study is provided in (*SI Appendix*, *Supplementary Materials and Methods*). A mouse model, named tg*Breaker*, which allows for inducible expression of the I-SceI nuclease, was generated. Cell culture, RNAi, histology and immunofluorescence staining, repair efficiency analysis, primary cardiomyocyte isolation, comet assay, co-IP, proximity ligation assay, subcellular fractionation, ChIP, qRT-PCR, echocardiography, transfection, virus infection, and CC and ISO injection were performed.

Data, Materials, and Software Availability. All study data are included in the article and/or *SI Appendix*.

ACKNOWLEDGMENTS. This work was supported by the National Key R&D Program of China (2022YFA1103700 and 2021YFA1102000 to Z.M. and 2018YFA0800104 and 2017YFA0105601 to K.W.), the National Natural Science Foundation of China (82225017, 32270750, and 82071565 to Z.M., 32070823 to K.W., 81972457 and 32171288 to Y.J., 32200595 to Y.C., and 92168205 to H.Z.), and the Shanghai Sailing Program (22YF1434300 to Y.C.). The working model was created with https://www.BioRender.com.

Author affiliations: [a]Shanghai Key Laboratory of Maternal Fetal Medicine, Clinical and Translational Research Center of Shanghai First Maternity and Infant Hospital, Frontier Science Center for Stem Cell Research, School of Life Sciences and Technology, Tongji University, Shanghai 200092, China; [b]Shanghai Key Laboratory of Signaling and Disease Research, School of Life Sciences and Technology, Tongji University, Shanghai 200092, China; [c]Institute for Regenerative Medicine, Shanghai East Hospital, Shanghai Institute of Stem Cell Research and Clinical Translation, Shanghai Key Laboratory of Signaling and Disease Research, Frontier Science Center for Stem Cell Research, School of Life Sciences and Technology, Tongji University, Shanghai 200092, China; [d]National Engineering Research Center for Biotechnology (Shenzhen), Carson International Cancer Center, Medical Research Center, Shenzhen University Health Science Center, Shenzhen 518055, China; and [e]Tsingtao Advanced Research Institute, Tongji University, Qingdao 266071, China

1. A. De Sandre-Giovannoli *et al.*, Lamin a truncation in Hutchinson-Gilford progeria. *Science* **300**, 2055 (2003).
2. M. Eriksson *et al.*, Recurrent de novo point mutations in lamin A cause Hutchinson-Gilford progeria syndrome. *Nature* **423**, 293–298 (2003).
3. R. C. Hennekam, Hutchinson-Gilford progeria syndrome: Review of the phenotype. *Am. J. Med. Genet. A* **140**, 2603–2624 (2006).
4. H. Y. Zhang, Z. M. Xiong, K. Cao, Mechanisms controlling the smooth muscle cell death in progeria via down-regulation of poly(ADP-ribose) polymerase 1. *Proc. Natl. Acad. Sci. U.S.A.* **111**, E2261–E2270 (2014).
5. S. Sun *et al.*, Vascular endothelium-targeted Sirt7 gene therapy rejuvenates blood vessels and extends life span in a Hutchinson-Gilford progeria model. *Sci. Adv.* **6**, eaay5556 (2020).
6. C. Lopez-Otin, M. A. Blasco, L. Partridge, M. Serrano, G. Kroemer, The hallmarks of aging. *Cell* **153**, 1194–1217 (2013).
7. F. De Majo *et al.*, Genomic instability in the naturally and prematurely aged myocardium. *Proc. Natl. Acad. Sci. U.S.A.* **118**, e2022974118 (2021).
8. B. H. Liu *et al.*, Genomic instability in laminopathy-based premature aging. *Nat. Med.* **11**, 780–785 (2005).
9. A. B. Redwood *et al.*, A dual role for A-type lamins in DNA double-strand break repair. *Cell Cycle* **10**, 2549–2560 (2011).
10. S. Gonzalo, R. Kreienkamp, DNA repair defects and genome instability in Hutchinson-Gilford Progeria Syndrome. *Curr. Opin. Cell Biol.* **34**, 75–83 (2015).
11. W. P. Roos, B. Kaina, DNA damage-induced cell death by apoptosis. *Trends Mol. Med.* **12**, 440–450 (2006).
12. F. d'Adda di Fagagna, Living on a break: Cellular senescence as a DNA-damage response. *Nat. Rev. Cancer* **8**, 512–522 (2008).
13. A. Vaidya *et al.*, Knock-in reporter mice demonstrate that DNA repair by non-homologous end joining declines with age. *Plos Genet.* **10**, e1004511 (2014).
14. D. G. Hardie, F. A. Ross, S. A. Hawley, AMPK: A nutrient and energy sensor that maintains energy homeostasis. *Nat. Rev. Mol. Cell Bio.* **13**, 251–262 (2012).
15. R. H. Moghaddam *et al.*, Natural AMPK activators in cardiovascular disease prevention. *Front. Pharmacol.* **12**, 738420 (2022).
16. R. M. Sniecinski, S. Wright, J. H. Levy, "Chapter 3 - Cardiovascular pharmacology" in *Cardiothoracic Critical Care*, D. Sidebotham, A. McKee, M. Gillham, J. H. Levy, Eds. (Butterworth-Heinemann, Philadelphia, 2007), pp. 33–52.
17. G. Olivetti, M. Melissari, J. M. Capasso, P. Anversa, Cardiomyopathy of the aging human heart - Myocyte loss and reactive cellular hypertrophy. *Circ. Res.* **68**, 1560–1568 (1991).
18. M. Sandri *et al.*, Foxo transcription factors induce the atrophy-related ubiquitin ligase atrogin-1 and cause skeletal muscle atrophy. *Cell* **117**, 399–412 (2004).
19. C. Skurk *et al.*, The FOXO3a transcription factor regulates cardiac myocyte size downstream of AKT signaling. *J. Biol. Chem.* **280**, 20814–20823 (2005).
20. O. A. Sedelnikova *et al.*, Senescing human cells and ageing mice accumulate DNA lesions with unrepairable double-strand breaks. *Nat. Cell Biol.* **6**, 168–170 (2004).
21. O. A. Sedelnikova *et al.*, Delayed kinetics of DNA double-strand break processing in normal and pathological aging. *Aging Cell* **7**, 89–100 (2008).
22. C. F. Wang *et al.*, DNA damage response and cellular senescence in tissues of aging mice. *Aging Cell* **8**, 311–323 (2009).
23. Z. Li *et al.*, Impaired DNA double-strand break repair contributes to the age-associated rise of genomic instability in humans. *Cell Death Differ.* **23**, 1765–1777 (2016).
24. A. Collins *et al.*, Measuring DNA modifications with the comet assay: A compendium of protocols. *Nat. Protoc.* **18**, 929–989 (2023).
25. Z. Y. Mao, M. Bozzella, A. Seluanov, V. Gorbunova, Comparison of nonhomologous end joining and homologous recombination in human cells. *DNA Repair* **7**, 1765–1771 (2008).
26. Z. Mao, M. Bozzella, A. Seluanov, V. Gorbunova, DNA repair by nonhomologous end joining and homologous recombination during cell cycle in human cells. *Cell Cycle* **7**, 2902–2906 (2008).
27. C. Wang *et al.*, Rational combination therapy for hepatocellular carcinoma with PARP1 and DNA-PK inhibitors. *Proc. Natl. Acad. Sci. U.S.A.* **117**, 26356–26365 (2020).
28. W. E. Louch, K. A. Sheehan, B. M. Wolska, Methods in cardiomyocyte isolation, culture, and gene transfer. *J. Mol. Cell Cardiol.* **51**, 288–298 (2011).
29. P. Alam, B. D. Maliken, M. J. Ivey, S. M. Jones, O. Kanisicak, Isolation, transfection, and long-term culture of adult mouse and rat cardiomyocytes. *J. Vis. Exp.* **164** (2020), 10.3791/61073.
30. W. Zhang *et al.*, A high-throughput small molecule screen identifies farrerol as a potentiator of CRISPR/Cas9-mediated genome editing. *Elife* **9**, e56008 (2020).
31. Y. Chen, Z. Cui, Z. Chen, Y. Jiang, Z. Mao, IDDoR: A novel reporter mouse system for simultaneous and quantitative in vivo analysis of both DNA double-strand break repair pathways. *Protein Cell* **14**, 369–375 (2022).
32. G. Feng *et al.*, Imaging neuronal subsets in transgenic mice expressing multiple spectral variants of GFP. *Neuron* **28**, 41–51 (2000).
33. S. Ghosh, B. Liu, Y. Wang, Q. Hao, Z. Zhou, Lamin A is an endogenous SIRT6 activator and promotes SIRT6-mediated DNA repair. *Cell Rep.* **13**, 1396–1406 (2015).
34. L. Onn *et al.*, SIRT6 is a DNA double-strand break sensor. *Elife* **9**, e51636 (2020).
35. W. Chen *et al.*, Sirt6 promotes DNA end joining in iPSCs derived from old mice. *Cell Rep.* **18**, 2880–2892 (2017).
36. R. A. McCord *et al.*, SIRT6 stabilizes DNA-dependent protein kinase at chromatin for DNA double-strand break repair. *Aging-Us* **1**, 109–121 (2009).
37. Y. Chen *et al.*, A PARP1-BRG1-SIRT1 axis promotes HR repair by reducing nucleosome density at DNA damage sites. *Nucleic Acids Res.* **47**, 8563–8580 (2019).
38. Z. Y. Mao *et al.*, SIRT6 promotes DNA repair under stress by activating PARP1. *Science* **332**, 1443–1446 (2011).
39. H. P. Liu *et al.*, Nuclear cGAS suppresses DNA repair and promotes tumorigenesis. *Nature* **563**, 131–136 (2018).
40. R. E. Kleiner, P. Verma, K. R. Molloy, B. T. Chait, T. M. Kapoor, Chemical proteomics reveals a gammaH2AX-53BP1 interaction in the DNA damage response. *Nat. Chem. Biol.* **11**, 807–814 (2015).
41. L. B. Schultz, N. H. Chehab, A. Malikzay, T. D. Halazonetis, p53 binding protein 1 (53BP1) is an early participant in the cellular response to DNA double-strand breaks. *J. Cell Biol.* **151**, 1381–1390 (2000).
42. M. P. Mallampalli, G. Huyer, P. Bendale, M. H. Gelb, S. Michaelis, Inhibiting farnesylation reverses the nuclear morphology defect in a HeLa cell model for Hutchinson-Gilford progeria syndrome. *Proc. Natl. Acad. Sci. U.S.A.* **102**, 14416–14421 (2005).
43. B. C. Capell *et al.*, Inhibiting farnesylation of progerin prevents the characteristic nuclear blebbing of Hutchinson-Gilford progeria syndrome. *Proc. Natl. Acad. Sci. U.S.A.* **102**, 12879–12884 (2005).
44. G. Obe, C. Johannes, D. Schulte-Frohlinde, DNA double-strand breaks induced by sparsely ionizing radiation and endonucleases as critical lesions for cell death, chromosomal aberrations, mutations and oncogenic transformation. *Mutagenesis* **7**, 3–12 (1992).
45. K. M. Frank *et al.*, DNA ligase IV deficiency in mice leads to defective neurogenesis and embryonic lethality via the p53 pathway. *Mol. Cell* **5**, 993–1002 (2000).
46. P. Bouwman, J. Jonkers, The effects of deregulated DNA damage signalling on cancer chemotherapy response and resistance. *Nat. Rev. Cancer* **12**, 587–598 (2012).
47. M. Bohgaki *et al.*, The E3 ligase PIRH2 polyubiquitylates CHK2 and regulates its turnover. *Cell Death Differ.* **20**, 812–822 (2013).

48. E. M. Kass *et al.*, Stability of checkpoint kinase 2 is regulated via phosphorylation at serine 456. *J. Biol. Chem.* **282**, 30311–30321 (2007).
49. N. J. Byrne, M. M. Sung, J. R. B. Dyck, "The role of AMPK in the control of cardiac hypertrophy" in *Cardiac Energy Metabolism in Health and Disease*, G. D. Lopaschuk, N. S. Dhalla, Eds. (Springer New York, New York, NY), 2014), pp. 199–220.
50. S. A. Hawley *et al.*, Characterization of the AMP-activated protein kinase kinase from rat liver and identification of threonine 172 as the major site at which it phosphorylates AMP-activated protein kinase. *J. Biol. Chem.* **271**, 27879–27887 (1996).
51. S. J. Park *et al.*, DNA-PK promotes the mitochondrial, metabolic, and physical decline that occurs during aging. *Cell Metab.* **25**, 1135–1146.e7 (2017).
52. G. H. Liu *et al.*, Recapitulation of premature ageing with iPSCs from Hutchinson-Gilford progeria syndrome. *Nature* **472**, 221–225 (2011).
53. B. E. Crute, K. Seefeld, J. Gamble, B. E. Kemp, L. A. Witters, Functional domains of the alpha1 catalytic subunit of the AMP-activated protein kinase. *J. Biol. Chem.* **273**, 35347–35354 (1998).
54. J. Bartek, J. Falck, J. Lukas, CHK2 kinase–a busy messenger. *Nat. Rev. Mol. Cell Biol* **2**, 877–886 (2001).
55. S. Matsuoka, M. Huang, S. J. Elledge, Linkage of ATM to cell cycle regulation by the Chk2 protein kinase. *Science* **282**, 1893–1897 (1998).
56. K. L. Arienti *et al.*, Checkpoint kinase inhibitors: SAR and radioprotective properties of a series of 2-arylbenzimidazoles. *J. Med. Chem.* **48**, 1873–1885 (2005).
57. S. A. Hawley *et al.*, Complexes between the LKB1 tumor suppressor, STRAD alpha/beta and MO25 alpha/beta are upstream kinases in the AMP-activated protein kinase cascade. *J. Biol.* **2**, 28 (2003).
58. E. L. Greer *et al.*, The energy sensor AMP-activated protein kinase directly regulates the mammalian FOXO3 transcription factor. *J. Biol. Chem.* **282**, 30107–30119 (2007).
59. D. R. Bolster, S. J. Crozier, S. R. Kimball, L. S. Jefferson, AMP-activated protein kinase suppresses protein synthesis in rat skeletal muscle through down-regulated mammalian target of rapamycin (mTOR) signaling. *J. Biol. Chem.* **277**, 23977–23980 (2002).
60. G. Zhou *et al.*, Role of AMP-activated protein kinase in mechanism of metformin action. *J. Clin. Invest.* **108**, 1167–1174 (2001).
61. C. Jian *et al.*, Low-dose sorafenib acts as a mitochondrial uncoupler and ameliorates nonalcoholic steatohepatitis. *Cell Metab.* **31**, 892–908.e811 (2020).
62. G. Kong *et al.*, AMPK controls the axonal regenerative ability of dorsal root ganglia sensory neurons after spinal cord injury. *Nat. Metab.* **2**, 918–933 (2020).
63. X. Z. Zhuo *et al.*, Isoproterenol instigates cardiomyocyte apoptosis and heart failure via AMPK inactivation-mediated endoplasmic reticulum stress. *Apoptosis* **18**, 800–810 (2013).
64. J. H. Yang *et al.*, Loss of epigenetic information as a cause of mammalian aging. *Cell* **186**, 305–326. e27 (2023).
65. V. Krishnan *et al.*, Histone H4 lysine 16 hypoacetylation is associated with defective DNA repair and premature senescence in Zmpste24-deficient mice. *Proc. Natl. Acad. Sci. U.S.A.* **108**, 12325–12330 (2011).
66. B. H. Liu *et al.*, Depleting the methyltransferase Suv39h1 improves DNA repair and extends lifespan in a progeria mouse model. *Nat. Commun.* **4**, 1868 (2013).
67. D. K. Shumaker *et al.*, Mutant nuclear lamin A leads to progressive alterations of epigenetic control in premature aging. *Proc. Natl. Acad. Sci. U.S.A.* **103**, 8703–8708 (2006).
68. G. Rona, C. I. Chappel, T. Balazs, R. Gaudry, An infarct-like myocardial lesion and other toxic manifestations produced by isoproterenol in the rat. *AMA Arch. Pathol.* **67**, 443–455 (1959).
69. M. R. Hamczyk, L. del Campo, V. Andres, Aging in the cardiovascular system: Lessons from Hutchinson-gilford progeria syndrome. *Annu. Rev. Physiol.* **80**, 27–48 (2018).
70. J. Ngo *et al.*, Bax deficiency extends the survival of Ku70 knockout mice that develop lung and heart diseases. *Cell Death Dis.* **6**, e1706 (2015).
71. L. Bee *et al.*, A nonsense mutation of human XRCC4 is associated with adult-onset progressive encephalocardiomyopathy. *EMBO Mol. Med.* **7**, 918–929 (2015).
72. S. E. Lipshultz *et al.*, Chronic progressive cardiac dysfunction years after doxorubicin therapy for childhood acute lymphoblastic leukemia. *J. Clin. Oncol.* **23**, 2629–2636 (2005).
73. N. Matsumura *et al.*, Co-administration of resveratrol with doxorubicin in young mice attenuates detrimental late-occurring cardiovascular changes. *Cardiovasc. Res.* **114**, 1350–1359 (2018).
74. M. S. Willis *et al.*, Doxorubicin exposure causes subacute cardiac atrophy dependent on the striated muscle-specific ubiquitin ligase MuRF1. *Circ. Heart Fail* **12**, e005234 (2019).
75. D. S. Chen, J. Yan, P. Z. Yang, Cardiomyocyte atrophy, an underestimated contributor in doxorubicin-induced cardiotoxicity. *Front. Cardiovasc. Med.* **9**, 812578 (2022).
76. L. B. Gordon *et al.*, Association of lonafarnib treatment vs. no treatment with mortality rate in patients with Hutchinson-gilford progeria syndrome. *JAMA* **319**, 1687–1695 (2018).
77. L. B. Gordon *et al.*, Impact of farnesylation inhibitors on survival in Hutchinson-Gilford progeria syndrome. *Circulation* **130**, 27–34 (2014).
78. B. S. Davies *et al.*, An accumulation of non-farnesylated prelamin A causes cardiomyopathy but not progeria. *Hum. Mol. Genet.* **19**, 2682–2694 (2010).
79. S. K. Park, O. S. Shin, Metformin alleviates ageing cellular phenotypes in Hutchinson-Gilford progeria syndrome dermal fibroblasts. *Exp. Dermatol.* **26**, 889–895 (2017).
80. A. L. Egesipe *et al.*, Metformin decreases progerin expression and alleviates pathological defects of Hutchinson–Gilford progeria syndrome cells. *NPJ Aging Mech. Dis.* **2**, 16026 (2016).
81. L. Nesti, A. Natali, Metformin effects on the heart and the cardiovascular system: A review of experimental and clinical data. *Nutr. Metab. Cardiovasc. Dis.* **27**, 657–669 (2017).